PCCP

PAPER

View Article Online
View Journal | View Issue

Cite this: *Phys. Chem. Chem. Phys.*, 2026, **28**, 6323

The destruction of $^3HeT^+$ in collisions with tritium: a dynamical study†

Jayakrushna Sahoo,[a] Duncan Bossion,[b] Felix Spanier,[c] Tomás González-Lezana *[d] and Yohann Scribano *[a]

Received 10th October 2025,
Accepted 3rd February 2026

DOI: 10.1039/d5cp03908h

rsc.li/pccp

The dynamics of the T + $^3HeT^+(v = 0, j = 0) \rightarrow T_2^+ + {}^3He$ reaction has been theoretically investigated by means of quantum, statistical and quasi-classical methods on a recently refined potential energy surface. Integral cross sections, rotational distributions, differential cross sections and rate constants have been obtained. The destruction following the above reaction of $^3HeT^+$, an ionic species formed during the single-β decay of the molecular tritium, is thus studied in detail, and its possible influence on current experiments to estimate the mass of the neutrino discussed. In this sense, values of the rate constant for such a process between 10 and 500 K have been predicted to be around 1.2×10^{-9} cm^3 s^{-1}. The thermal rate constant, obtained by considering also the rates for the processes initiated from the five first rotational states $^3HeT^+(v = 0, j = 1–5)$, confirms such a value.

1 Introduction

The $^3HeT^+$ ionic species is a product of the single-β decay of molecular tritium:

$$T_2 \rightarrow {}^3HeT^+ + e^- + \bar{\nu}_e \quad (1)$$

the main process exploited for recent estimates of the neutrino mass by the KArlsruhe TRItium Neutrino (KATRIN) experiment.[1,2] The KATRIN experiment consists of a windowless gaseous tritium source where a constant inflow of molecular tritium, T_2, provides a stable rate of β-decay electrons. These electrons are transported by means of a strong guide magnetic field to the detector and can interact with the ambient gas *via* ionization recombination, clustering and elastic scattering.[3] The result of these atomic and molecular processes is the production of secondary particles which may subsequently yield even more particles which end either eliminated *via* recombination processes or absorbed by the walls of the experiment. With a sufficiently large charged particle density a plasma is finally formed in the source of the apparatus. The plasma generates an electrostatic potential which may change the energy of decaying tritium with respect to the detector. Some of the relevant processes occurring under such conditions have been simulated by means of a Monte Carlo model.[4]

Within the conditions of the KATRIN experiment, such as characteristic temperatures of about 80 K and flow equilibrium of the ambient gas, tritium clustering is the dominant process, with higher densities of T_3^+ and T_5^+ than those for T^+ and T_2^+. The abundance of larger clusters can be relevant but the cross sections for their actual formation are unknown to date. Upcoming versions of the tritium-decay based experiments, such as the so called Project 8 experiment,[5] are now in a preliminary stage where the operating conditions and parameters are being carefully tested. Among the most significant novelties introduced in this new set up with respect to the original apparatus, we find that the desired temperature range is significantly much lower (coming down to the millikelvin range). Moreover, the injected atomic tritium stays far longer in the source than before. These changes lead to a number of different atomic and molecular processes becoming important. In particular $^3He^+$ is also expected to play some role since helium is not removed from the source. The existing tritium can then collide first with ionic helium to form $^3HeT^+$ and then with this species itself, $T + {}^3HeT^+$. Although this process is not crucial for the actual observation of the neutrino, constituents like $^3HeT^+$ and T_2 have significantly different cross sections for ionization and recombination which in turn have an impact on the total electron content and the plasma properties.

This current need for relevant information regarding the possible processes occurring among the existing molecular

[a] *Laboratoire Univers et Particules de Montpellier, Université de Montpellier, UMR-CNRS 5299, 34095 Montpellier Cedex, France. E-mail: yohann.scribano@umontpellier.fr*
[b] *IPR—Université de Rennes Bât 11b, Campus de Beaulieu, 263 Avenue du Général Leclerc, 35042 Rennes Cedex, France*
[c] *Institut für Theoretische Astrophysik, Universität Heidelberg, Albert-Ueberle-Str. 2 und Philosophenweg 12, 69120 Heidelberg, Germany*
[d] *Instituto de Física Fundamental, IFF-C.S.I.C., Serrano 123, Madrid 28006, Spain. E-mail: t.gonzalez.lezana@csic.es*

† Part of the Festschrift honouring Prof. N. Sathyamurthy's 75th birthday.

species in the above described experiments leads us to address the destruction of $^3HeT^+$ *via* the following reaction (^{3}He/T):

$$T + {}^3HeT^+ \rightarrow T_2{}^+ + {}^3He \quad (2)$$

As with many other processes including tritium (or ^{3}He) neither theoretical calculations nor experimental observations exist or can be trivially derived from ^{1}H and ^{4}He. This makes precision calculations for tritium experiments rather complicated. As Project 8 is still in the design phase, it is possible to build a theoretical model for which adequate observational tools can be developed.

In a recent work,[6] some of us have investigated the dynamics of the isotopic version (^{4}He/H) of the reaction in eqn (2) in which tritium is substituted by usual hydrogen, H, and ^{3}He is replaced by ^{4}He. Given the relevance of the HeH^+ ionic species within an astrophysical context, the $H + {}^4HeH^+ \rightarrow H_2{}^+ + {}^4He$ reaction has been the subject of numerous investigations. Many of these previous studies[7–15] had employed the potential energy surface (PES) reported in ref. 16 and subsequent analytical fits. However, as shown by Sahoo *et al.*,[6] the PES developed by Ramachandran *et al.*[16] presents an ''artificial barrier'' on the reaction path as a spurious result of the numerical fitting procedure. The dynamics of the reaction was investigated in ref. 6 with a correct long-range interaction by means of a time independent quantum method (TIQM), a statistical quantum method (SQM) and quasi-classical trajectory (QCT) calculations. The resulting integral cross sections (ICSs) exhibited a monotonic increase as the collision energy decreases as opposed to the abrupt non-Langevin decrease found using the original PES.[15] The corresponding rate constants calculated on the new PES exhibited a noticeable enhancement at low temperatures which surely would affect the abundance of HeH^+ in the early stages of the universe predicted by astrophysical models. This newly corrected PES was also employed in a subsequent calculation[17] for a variant of the title reaction where one of the H atoms is substituted by deuterium (^{4}He/D): $HeH^+ + D \rightarrow HD^+ + He$ and a good agreement with the experimental cross sections established the validity of the new surface. This corrected PES was also considered as the benchmark to test the performance of a mixed kernel/neural network representation of a reactive PES for the H_2He^+ system.[18]

In this work we have followed a similar procedure to study the dynamics of the reaction (^{3}He/T) in eqn (2), and calculations by means of the above mentioned TIQM, SQM and QCT approaches have been conducted on the corrected PES reported in ref. 6. Both, the above mentioned methods and the PES employed are briefly described in Section 2.

2 Theoretical methods

2.1 Potential energy surface

The description of the procedure to obtain a corrected version of the Ramachandran PES[16] was given in ref. 6 and its supplementary information (SI), so here we will restrict ourselves to provide the most relevant details. Originally, Ramachandran *et al.* developed three different surfaces by calculating *ab initio* energy points by means of both multi-reference[19,20] and full configuration interaction.[21,22] methods and correlation-consistent polarized valence quadruple (cc-pVQZ)- and quintuple-zeta (cc-pV5Z) basis sets.[23] These electronic energies were then analytically fitted using Aguado–Paniagua[24] functions with polynomials of different highest order (6 and 8). The correction proposed by Sahoo *et al.*[6] manages to remove the spurious barrier existing in the PES by Ramachandran *et al.* by describing, on the one hand, the three-body terms with an analytical Aguado–Paniagua fitting of FCI/cc-pVQZ *ab initio* energy points and, on the other hand, the two-body terms by means of Aguado–Paniagua[24] polynomials (order 10) and long-range terms taken from Koner *et al.*[25]

2.2 Time independent quantum method

The quantum scattering dynamics of the reaction is investigated using the TIQM scattering method, as implemented in the ABC quantum reactive program by Skouteris *et al.*[26] The method employs a coupled-channel hyperspherical coordinate approach to solve the time-independent Schrödinger equation on a single adiabatic electronic PES for the nuclear motion of a triatomic reactive system. The resulting set of coupled-channel hyperradial equations is then solved using the constant reference potential log-derivative method.[27] At the end of the propagation, the scattering matrix (*S*-matrix) is obtained by imposing asymptotic boundary conditions at large hyperradius. Those scattering matrix elements are computed over a specified range of total energy E (in a single run) for a given total angular quantum number J and triatomic parity eigenvalue across all three arrangement channels (inelastic, exchange and reactive channels). Next, the parity-adapted *S*-matrix elements are appropriately combined to obtain the helicity-representation *S*-matrix elements, $S^J_{vj\Omega\rightarrow v'j'\Omega'}(E)$, (see eqn (1) and (2) of ref. 26) in order to get the reaction observables such as cross sections and rate constants. The reactive state-to-state cross section is calculated according to

$$\sigma_{vj\rightarrow v'j'}(E) = \frac{\pi}{\tilde{k}_{vj}{}^2(2j+1)} \sum_{J=0}^{J_{max}} \sum_{\Omega,\Omega'} (2J+1) P^J_{vj\Omega\rightarrow v'j'\Omega'}(E) \quad (3)$$

where the reaction probability $P^J_{vj\Omega\rightarrow v'j'\Omega'}(E) \equiv \left|S^J_{vj\Omega\rightarrow v'j'\Omega'}(E)\right|^2$ and $\tilde{k}_{vj} = \sqrt{2\mu E_c}/\hbar$, with μ being the atom–diatom reduced mass of the reactant channel, and E_c being the collision energy which is the total energy minus the rovibrational energy of the reactant diatom. The symbols v, j, and Ω denote the vibrational, rotational, and helicity quantum numbers of the reactant channel, respectively, and the corresponding primed quantities are those for the product channel.

Formally, the state-to-state temperature dependent rate coefficients are related to the corresponding cross sections by thermal averaging over a Maxwell–Boltzmann velocity distribution according to

$$k_{vj\rightarrow v'j'}(T) = \sqrt{\frac{8k_BT}{\pi\mu}} \frac{1}{(k_BT)^2} \int E_c \sigma_{vj\rightarrow v'j'}(E_c) e^{-E_c/k_BT} dE_c. \quad (4)$$

The numerical integration is performed as presented in ref. 6. From those state-to-state observables it is then possible to easily determine initial state observables or thermal average observables.

In addition, we have obtained differential cross sections (DCSs) as a function of the energy and the scattering angle θ obtained by means of the following expression:[26]

$$\sigma_{vj\Omega\to v'j'\Omega'}(E,\theta)=\left|\frac{1}{2i\tilde{k}_{vj}}\sum_J(2J+1)d_{\Omega\Omega'}(\theta)S^J_{vj\Omega,v'j'\Omega'(E)}\right|^2. \quad (5)$$

Performing these TIQM calculations requires the input of several parameters, the values of which are determined by means of convergence tests. For example, several convergence tests at total angular momentum $J = 0$ are performed in order to get the final optimal values of said parameters. In Table S1 of the SI specific parameters used for the generation of reaction cross sections with the ABC code are listed. Extensive convergence tests are carried out for all parameters in each E_c range as given in Table S1 of the SI. The convergence of the cross section is checked with respect to the maximum number of rotational states in any reactive channel (j_{max}), the maximum total energy that includes all open and closed rovibrational levels in the basis set (E_{max}), the maximum value of the hyperradius (ρ_{max}), the number of log derivative propagation sectors (n_{sec}), the helicity truncation parameter (Ω_{max}) and the maximum total angular momentum (J_{max}).

2.3 Statistical quantum method

The SQM was described in the previous investigation of the H + $^4HeH^+ \rightarrow H_2^+ + {}^4He$ reaction.[6] The method was designed by Manolopoulos and collaborators[28,29] to treat atom–diatom complex-forming reactions and it has been employed on numerous occasions (an early review with some applications can be found in ref. 30). Within such an assumption for the overall dynamics of the process, the state-to-state probability can be expressed as:

$$\left|S^J_{\alpha,\beta}(E)\right|^2=P^J_{\alpha,\beta}(E)\approx\frac{p^J_\alpha(E)p^J_\beta(E)}{\sum_l p^J_l(E)}, \quad (6)$$

where J is the total angular momentum, $p^J_\alpha(E)$ is the capture probability for the intermediate complex formation from the initial $\alpha = (v, j)$ rovibrational states of the reactants $^3HeT^+(v, j)$, $p^J_\beta(E)$ is the probability for the collision complex to fragment onto the final $\beta = (v', j')$ rovibrational states of the products $T_2^+(v', j')$, and in the denominator the l index runs for all energetically accessible rovibrational states either in the reactants channel or the products channel at the energy value E. The capture probabilities of the above eqn (6) are obtained by solving the corresponding coupled channel equations[29] using a time independent log derivative method between the asymptotic region defined by R_{max} and the region where the intermediate complex is assumed to form, defined by the capture radius R_c. Numerical values for these R_c and R_{max} are 1.5 and 44.3 Å, respectively, for both reactants and product arrangements.

The above expression for the state-to-state reaction probability shown in eqn (6) is then used to calculate ICSs as indicated in eqn (3), which enable us to obtain as well rate coefficients following eqn (4). The calculation of DCSs, on the contrary, requires an extra approximation as explained in ref. 29, given that the SQM does not provide information on the phase of the scattering matrix. Thus, the adequate expression is given by:[29]

$$\sigma_{vj\Omega\to v'j'\Omega'}(E,\theta)\approx\frac{1}{8\tilde{k}_{vj}{}^2}\sum_J(2J+1)^2|d_{\Omega\Omega'}(\theta)|^2P^J_{vj\Omega,v'j'\Omega'(E)}. \quad (7)$$

2.4 Quasi-classical trajectory method

The QCT method is presented in detail in Truhlar & Muckerman[31] and here we only give a brief description. The internal energy associated to the diatomic initial state (v, j) matches that of the exact rovibrational energy of the state of interest, obtained using the Fourier grid Hamiltonian method.[32] The nuclear dynamics is performed by solving the classical Hamilton's equations (by means of a standard Runge–Kutta integrator with adaptive time stepsize) on the ground-state electronic PES.[6] At the end of the propagation, a set of continuous pseudo quantum numbers (rotational and vibrational) is obtained within the WKB approximation.[33] We then determine discrete quantum numbers (v', j') to which each trajectory is assigned through a binning procedure.[31] Within this work, we use our own modified version of the Gaussian binning (GB). The efficiency of this scheme was already highlighted in a previous study of H + $^4HeH^+ \rightarrow H_2^+ + {}^4He$ reaction.[15]

Each trajectory belongs to a histogram or Gaussian bin labeled (v', j'). The ensemble of trajectories allows us to determine the reactive state-to-state cross section as

$$\sigma_{vj\to v'j'}(E_c)=\pi b_{max}{}^2(E_c)P_{vj\to v'j'}(E_c) \quad (8)$$

where $P_{vj\to v'j'}(E_c)$ is the reaction probability determined by the ratio of the weight of reactive trajectories in the bin (v',j') by the total weight of all the trajectories (each trajectory has a weight of $w \leq 1$, based on the value of its pseudo quantum number, in our GB scheme as presented in ref. 15). Convergence of the maximum impact parameter $b_{max}(E_c) \equiv b_{max}(E_c;v, j)$ for each collisional energy is obtained by running small batches of trajectories beforehand, leading to maximal impact parameters between 8.7 and 67.6a_0 for the energy range considered. Cross-sections are computed with collision energies starting from 1×10^{-5} eV up to 1 eV. To account for the logarithmic behaviour of the cross section, we considered a logarithmic energy grid, with 5 energies per order of magnitude. Up to $N_t = 40\,000$ trajectories were propagated to minimize the standard deviation of the cross-section.

To estimate the lifetime of the intermediate complex for this chemical reaction, we determine a lifetime (or collision time) for each trajectory (labelled by α) at each collisional energy E_c and for the initial rovibrational state ($v = 0, j = 0$). This lifetime is the time during which the internuclear distances of all the

atoms are less than $5a_0$ during the collision. An average over all trajectories is then performed to obtain the average lifetime $\tau_{complex}$ of the complex as:

$$\tau_{complex}(E_c) = \frac{1}{N_t}\sum_{\alpha=1}^{N_t}\tau_\alpha \quad (9)$$

where N_t is the total number of propagated trajectories and τ_α is the lifetime of the αth trajectory. Values for the parameters used in the QCT calculation are shown in Table S2 of the SI.

3 Results and discussion

3.1 Integral cross sections and rate constants

In Fig. 1, we show the comparison among the ICSs obtained with the different methods discussed in Section 2 for the T + ^{3}HeT$^+$(v = 0, j = 0) → T_2^+ + ^{3}He reaction in an energy range up to 1.0 eV. The trend followed as the energy increases is a monotonic decrease. This was also the behavior observed in ref. 6 for the isotopic variant H + ^{4}HeH$^+$(v = 0, j = 0) → H_2^+ + ^{4}He; in fact the SQM ICSs obtained for that process is also included here in Fig. 1 for comparison (in the SI we include a version of this figure separated in log-scale energy decades; see Fig. S1). The agreement with the TIQM results of the SQM and QCT predictions is remarkable, with only slight differences at the low energy range ($\sim 10^{-5}$ eV). The apparent similarities of the present ICSs for the ^{3}He/T process in comparison with the corresponding ^{4}He/H reaction is consistent with a similar comparison established with the HeH$^+$ + D → HD$^+$ + He reaction.[17]

Rate constants have been calculated with these ICSs for the T + ^{3}HeT$^+$(v = 0, j = 0) → T_2^+ + ^{3}He reaction using eqn (4).

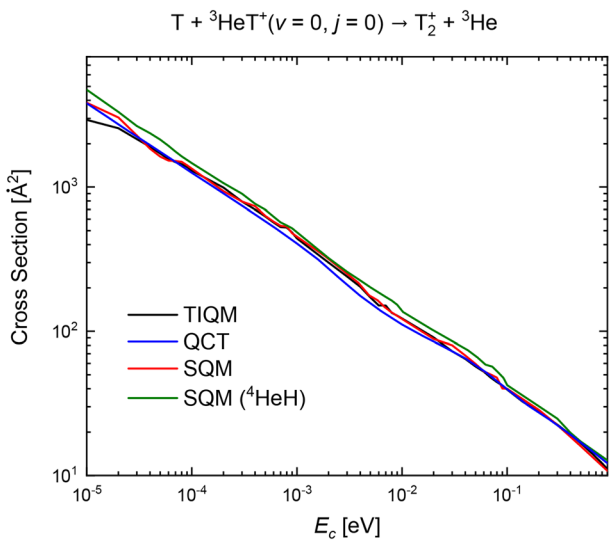

Fig. 1 Total integral cross section of the T + ^{3}HeT$^+$(v = 0, j = 0) → T_2^+ + ^{3}He as a function of the collisional energy obtained with the present theoretical methods (see Section 2): TIQM (black line), SQM (red line) and QCT approaches (blue line). The SQM result (green line) for the isotopic variant of the title reaction where H instead of T and ^{4}He instead of ^{3}He are considered[6] is included for comparison.

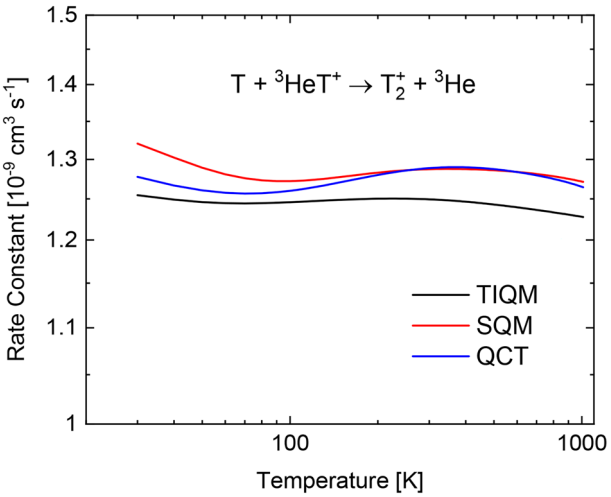

Fig. 2 Rate constants, $k(T)$, for the T + ^{3}HeT$^+$(v = 0, j = 0) → T_2^+ + ^{3}He reaction as a function of the temperature obtained with the TIQM (black line), SQM (red line) and QCT (blue line) methods.

Results are shown in Fig. 2 between T = 10 and 1000 K. The output from these three methods compare very well. In particular, the apparent capabilities of the statistical technique thus seem to support the hypothesis of a complex-forming mechanism leading the overall dynamics of the reaction that the ICSs shown in Fig. 1 suggest.

In Table 1 we show the numerical values of the $k(T)$ here obtained with the TIQM, SQM and QCT calculations at some specific temperatures. The agreement among the three sets of data is very good. The table also contains the comparison with the $k(T)$ reported in ref. 6 in our previous study on the H + ^{4}HeH$^+$(v = 0, j = 0) → H_2^+ + ^{4}He reaction. The order of magnitude of both isotopic variants of the reactive collision is the same (below 2.5 × 10^{-9} cm^3 s^{-1}) and in both cases the statistical prediction remains slightly above the TIQM values.

In order to provide some insight to a possible experimental investigation of the reaction, we have extended our study to other rovibrational states of the initial reactant ^{3}HeT$^+$(v, j) which may be populated at the temperatures under consideration. Thus, cross sections for the reaction initiated from the rotationally excited ^{3}HeT$^+$(v = 0, j = 1–5) states have been calculated by means of the computationally less expensive QCT and SQM methods. Results are shown in Fig. S2 and S3 of the SI. The corresponding rate constants obtained with them

Table 1 Rate constants $k(T)$ for the title reaction in comparison with those for the isotopic variant H + ^{4}HeH$^+$(v = 0, j = 0) → H_2^+ + ^{4}He reported in ref. 6 at specific values of the temperature obtained with the TIQM, SQM and QCT approaches. Units for the rate constants are 10^{-9} cm^3 s^{-1}

	^{3}He/T (this work)			^{4}He/H (ref. 6)		
T (K)	TIQM	SQM	QCT	TIQM	SQM	QCT
50	1.25	1.28	1.26	2.01	2.21	2.00
100	1.26	1.27	1.26	2.04	2.21	1.96
250	1.25	1.28	1.29	2.10	2.25	2.03
500	1.24	1.29	1.29	2.09	2.17	2.08

(shown in Fig. S4 and S5 of the SI) reveal that values do not vary too much from 1.2×10^{-9} cm^3 s^{-1} for all the initial rotational states under consideration in the case of the QCT and between 1.0 and 1.5×10^{-9} cm^3 s^{-1} in the case of the SQM predictions. Thermal rate constants obtained for both SQM and QCT methods by means of the expression $k(T) = e^{-E_j/k_B T} k_j(T) \Big/ \sum_j e^{-E_j/k_B T}$, where j stands for the corresponding $v = 0$, $j = 0$–5 rovibrational state, are compared in Fig. S6 of the SI. We can conclude that the destruction rate of $^3HeT^+$ is not significantly varied by its possible rotational excitation.

3.2 The dynamics of the reaction

The above results presented in Section 3.1 have given us an idea of how efficient and fast the title reaction is, in order to analyse its possible relevance in the context of experiments discussed in the introduction. As in other similar studies the observed agreement between the statistical predictions and the other theoretical methods employed here, especially the quantum mechanical (QM) ABC approach, can be interpreted as an indication that the overall dynamics of the process is governed by complex-forming mechanisms (since, as explained in Section 2.3, these techniques are specially designed to describe these kinds of insertion dynamics). We further investigate this possibility by analyzing the cross sections at the state-to-state level. We start with the final vibrational state selected ICSs obtained by means of the three theoretical approaches, which are shown in Fig. 3. Cross sections for $T_2^+(v' = 0)$ are smaller than for any other final vibrational state according to the TIQM (in the top panel) and the QCT (in the bottom panel) approaches, or in other words, $T_2^+(v')$ is mainly produced with some vibrational excitation in the entire energy range under study. SQM predictions indicate just the opposite. In fact, as expected from a statistical analysis, the increase in the vibrational excitation of $T_2^+(v' > 0)$ is accompanied by a decrease in the corresponding ICS. The TIQM values, in turn, show some mixing of final vibrational states as the energy increases. On the other hand the progression of the final v'-selected ICSs obtained in the QCT calculation goes from the $v' = 0$ case up to $v' = 3$ with some mixing too as the energy gets larger. The energy distribution among the possible different vibrational states in the product $T_2^+(v')$ species indicates thus deviation from the expected behaviour in a purely statistical dynamics.

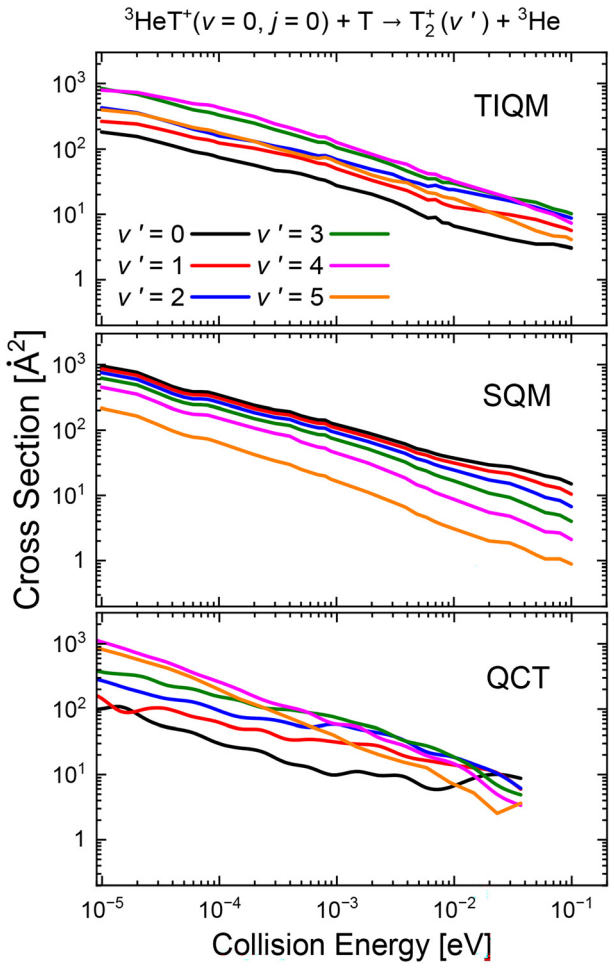

Fig. 3 Final vibrational state selected integral cross sections (in Å^2) as a function of the collision energy for the T + $^3HeT^+(v = 0, j = 0) \rightarrow T_2^+(v') + {}^3He$ reaction. TIQM results (top panel) are compared with SQM (middle panel) and QCT cross sections (bottom panel).

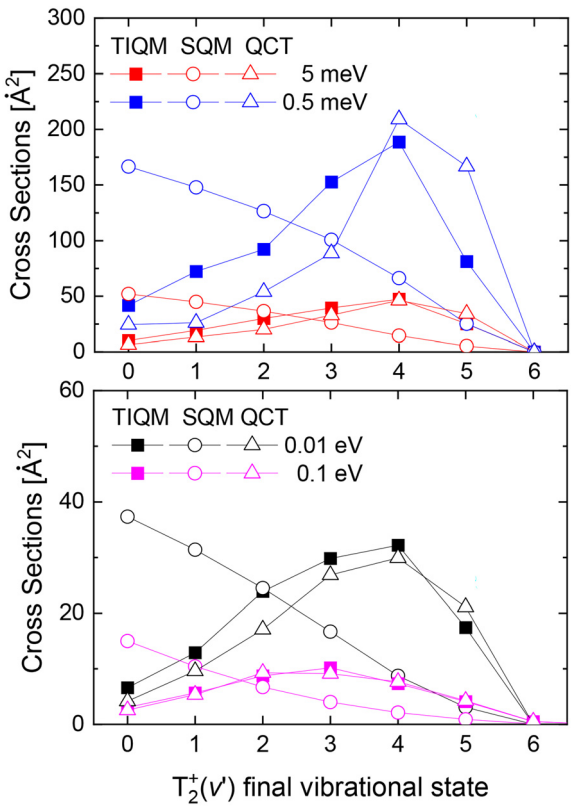

Fig. 4 Vibrational distributions (in Å^2) at four values of the collision energy, E_c = 0.5 meV (blue) and 5 meV (red) in the top panel and 0.01 eV (black) and 0.1 eV (magenta) in the bottom panel, obtained with the TIQM (filled squares), SQM (open circles), and QCT (open triangles) approaches for the T + $^3HeT^+(v = 0, j = 0) \rightarrow T_2^+(v') + {}^3He$ reaction.

An alternative way to visualize the specific distribution in the final vibrational manifold of the product T_2^+ is to consider fixed values of the collision energy. In Fig. 4, for example, we show vibrational distributions of the final state for the T + $^3HeT^+(v = 0, j = 0) \rightarrow T_2^+(v') + {}^3He$ reaction at different values of the collision energy. In almost all cases, the most favored vibrational state in the TIQM calculation is the $v' = 4$, something which in principle is at odds with the monotonic decrease predicted by statistical techniques of the cross section as the final v' state increases. QCT results, in contrast, manages to describe well such an inversion observed in the QM distributions. When the energy increases up to 0.1 eV, the largest population is found for $v' = 3$, a feature that the QCT calculation also reproduces. Thus the sequence presented in Fig. 4 suggests that a certain shift in the dynamics of the reaction may be occurring as the energy increases.

It is hard to point out a conclusive explanation for this inversion in the final vibrational distributions. Previous investigations of reactions such as F + H_2 reported that the dominant product was vibrationally excited HF($v' > 0$), as a result of the existence of QM reactive scattering resonances,[34] but this seems not to be the case for the title reaction. Interestingly, the study by Martínez *et al.*[35] concluded that vibrational distributions for O + $H_2^+(v = 0, j = 0) \rightarrow H + OH^+$ were inverted but not for O + $H_2^+(v = 0, j = 0) \rightarrow H^+ + OH$. Despite some possible explanations for this feature being given in terms of the properties of the ground and excited PES, the authors stated that: "*(. . .) it is far from trivial to determine the weight of these factors in the resulting distributions*".

In order to get insight into the ultimate origin of the deviations from a statistical description of the process, we have extracted state-to-state rotational distributions for the T + $^3HeT^+(v = 0, j = 0) \rightarrow T_2^+(v', j') + {}^3He$ reaction. Thus in Fig. 5 we present such a distribution for $E_c = 5 \times 10^{-3}$ eV (see Fig. S7 of the SI for the corresponding distribution at 0.01 eV). The population predicted for $v' = 0$–2 by the SQM is larger than the TIQM result. In view of the distributions shown in Fig. 5, the population of the low rotational levels for the vibrational ground and first excited $T_2^+(v' = 0, 1, j')$ states according to the statistical prediction is clearly overestimated: both TIQM and QCT results yield much hotter rotational distributions. The reason is that for the QM calculation, most of the lowest rotational states are almost unpopulated. A similar situation is observed for a higher collision energy, $E_c = 0.01$ eV, as shown in Fig. S1 of the SI.

The interesting thing is that, despite this different energy distribution among the final vibrational states, the overall

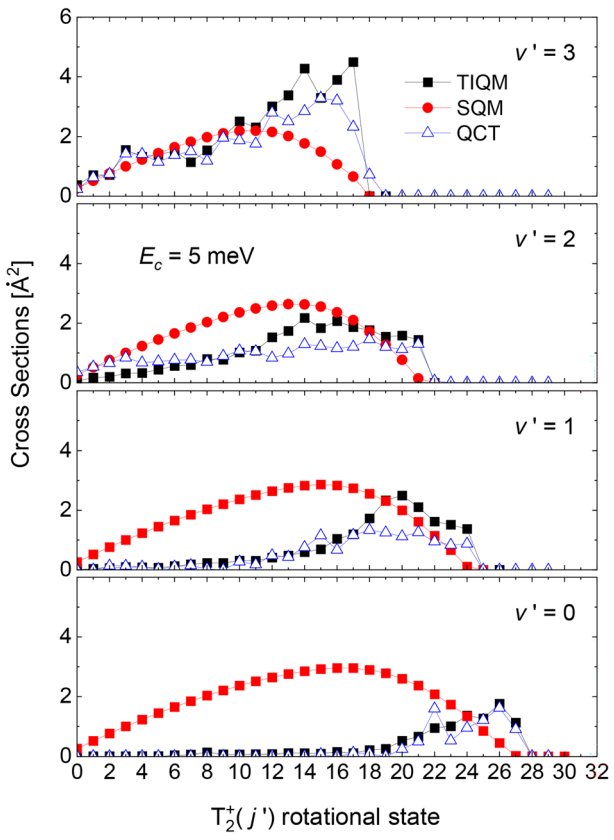

Fig. 5 Rotational distributions (measured in Å^2) at $E_c = 5 \times 10^{-3}$ calculated with the TIQM (black squares), SQM (red circles) and QCT (blue triangles) approaches for the T + $^3HeT^+(v = 0, j = 0) \rightarrow T_2^+(v' = 0–3, j') + {}^3He$ reaction.

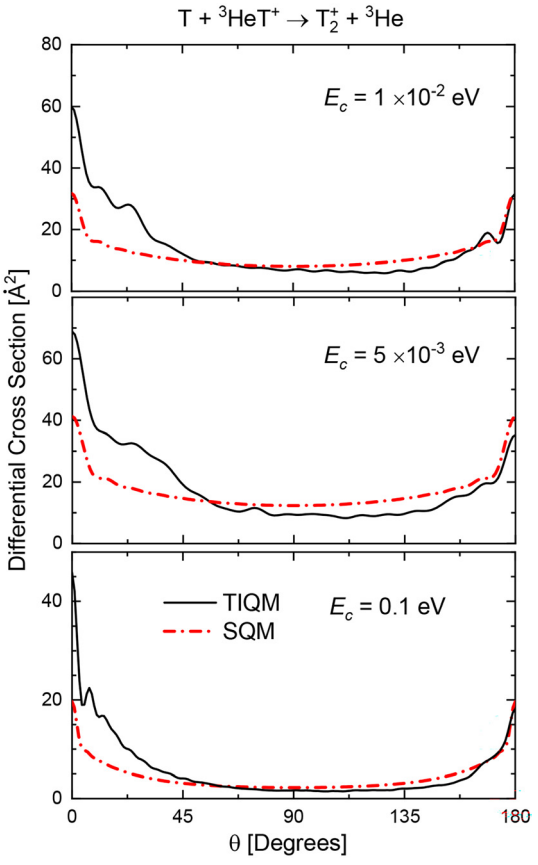

Fig. 6 Differential cross sections at different values of the collision energy ($E_c = 0.01$ (top), 5×10^{-3} (middle) and 0.1 eV (bottom panel)), obtained with the TIQM (solid black line) and SQM (dotted-dashed red line) approaches for the T + $^3HeT^+(v = 0, j = 0) \rightarrow T_2^+ + {}^3He$ reaction.

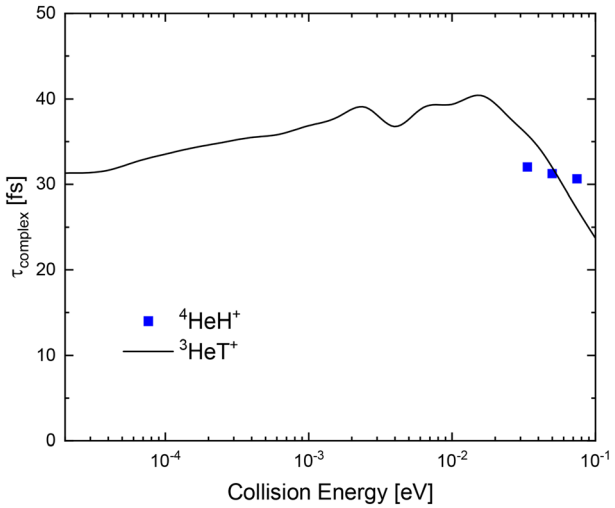

Fig. 7 Average intermediate complex lifetime, $\tau_{complex}$, defined in eqn (9), for the title reaction, T + $^3HeT^+$ (black solid line), compared to that of its isotopic counterpart, H + $^4HeH^+$ (blue squares) from ref. 15, as a function of the collisional energy.

quantities, once summed up over all the final rovibrational states, can be described by statistical means. An additional confirmation of this phenomenon comes with the analysis of the DCSs. The comparison between total DCSs at different energies reveals that some of the TIQM features are fairly well described by a statistical analysis. Fig. 6 shows results at E_c = 5, 10 meV and 0.1 eV, respectively. The QM distributions depart from a strict forward–backward symmetry, an indication of an overall dynamics which is not completely governed by complex-forming mechanisms. However, it is worth mentioning that the SQM correctly describes the TIQM distributions at both sideways direction ($\theta \sim 90^\circ$) and at least one of the peaks (in this case the backwards direction, 180°). As expected from the above discussion, differences with respect to the TIQM results become evident when we analyze state-to-state DCSs. Fig. S8 of the SI shows TIQM and SQM DCSs for the T + $^3HeT^+(v = 0, j = 0) \rightarrow T_2^+(v', j') + {}^3He$ process at 10 meV collision energy. As seen in the case of the ICSs, both sets of results are quantitatively equivalent (with the exception of the already mentioned preference seen along the forward direction $\theta \sim 0^\circ$) but the predictions for each final v' state are different.

Although for some other systems, such as H_3^+,[36] certain deviations from purely statistical predictions have been found at the state-to-state level despite the overall good description provided for total averaged magnitudes, the present findings suggest more intrinsic differences regarding the energy distribution among the available rovibrational degrees of freedom of the product diatom $T_2^+(v', j')$.

Finally, in an attempt to give some insight about the role played by possible complex-forming mechanisms, we use the QCT methodology to evaluate the complex lifetime as described in the Theoretical methods section. The average complex lifetime $\tau_{complex}$ as defined in eqn (9) is presented in Fig. 7. It fluctuates around 30 fs for collision energies between 10^{-5} and 2×10^{-2} eV, with a maximum of 40 fs at 10^{-2} eV, then drops towards lower values for higher collision energies. For comparison, above 10^{-2} eV, the complex lifetime for the isotopic reaction, H + $^4HeH^+$ extracted from ref. 15, is presented. This isotopic reaction was studied on the previous PES mentioned in the introduction, which is known to exhibit a wrong behavior at low energy due to the presence of an artificial barrier, and hence we only here consider collision energies not affected by this PES artifact. We can see that the complex lifetime of the two isotopic reactions are relatively similar. An additional QCT calculation on the ^{4}He/H reaction to study the vibrational distribution of the product (not shown here) confirms a similar deviation for both isotopic reactions from the statistical behavior regarding the distribution of vibrational states of the product.

4 Conclusions

We have performed a detailed investigation of the T + $^3HeT^+(v = 0, j = 0) \rightarrow T_2^+ + {}^3He$ reaction by means of a TIQM method combined with both SQM and QCT approaches. Total cross sections and rate constants are found not to differ significantly from previous results obtained for the isotopic variant ^{4}He/H reported in a previous communication.[6] Fine details of the dynamics of the reactions have been analyzed by calculating vibrational and rotational distributions at the state-to-state level specifying the final $T_2^+(v', j')$ rovibrational states, where deviations from a purely statistical behaviour have been observed. The slight asymmetry seen for DCSs where the forward scattering direction is favored seems to confirm the role played by direct mechanisms in the overall dynamics of the reaction. Despite these differences, total cross sections and rate constants, where results are summed up over all final rovibrational states, are fairly well described by statistical means. The growing precision of neutrino mass measurements requires an ever improving knowledge of the tritium chemistry network and the present study uncovers a new channel for tritium chemistry in experiments like KATRIN and Project-8. With calculations for the cross sections, such as those we report here, it is possible to determine the equilibrium concentration of $^3HeT^+$ a quantity which may be accessible in observations. This not only improves the precision of plasma chemistry calculations, it also allows for cross-checking calculations.

Author contributions

Jayakrushna Sahoo: conceptualization (supporting); data curation (lead); formal analysis (equal); funding acquisition (equal); investigation (lead); methodology (equal); resources (equal); software (equal); validation (equal); writing – original draft (equal); writing – review and editing (equal). Duncan Bossion: conceptualization (supporting); data curation (lead); formal analysis (lead); funding acquisition (equal); investigation (supporting); methodology (equal); resources (equal); software (equal); validation (equal); writing – original draft (equal); writing – review and editing (equal). Felix Spanier: conceptualization (supporting); data curation (supporting); formal analysis (supporting); funding

acquisition (supporting); investigation (supporting); methodology (supporting); resources (supporting); software (supporting); validation (supporting); writing – original draft (supporting); writing – review and editing (supporting). Tomás González Lezana: conceptualization (lead); data curation (lead); formal analysis (lead); funding acquisition (lead); investigation (lead); methodology (lead); resources (equal); software (equal); validation (equal); writing – original draft (lead); writing – review and editing (lead). Yohann Scribano: conceptualization (equal); data curation (supporting); formal analysis (supporting); funding acquisition (lead); investigation (supporting); methodology (equal); resources (supporting); software (supporting); validation (supporting); writing – original draft (equal); writing – review and editing (equal).

Conflicts of interest

The authors do not have conflicts to declare.

Data availability

The data that support the findings of this study are available as supplementary information (SI) with (a) values of the parameters for the ABC and QCT calculations; (b) Integral cross section (ICS) as a function of the energy obtained with the three methods for the T + ^{3}HeT($v = 0, j = 0$)$^+$ → T_2^+ + ^{3}He reaction; (c) ICSs for the reaction initiated from ^{3}HeT($v = 0, j = 0$–5)$^+$ obtained with the QCT and SQM methods; (d) rate constants for these same processes obtained with the QCT and SQM methods; (e) thermal rate constants obtained with rates for those initial states obtained with the QCT and SQM methods and finally (f) rotational distributions and differential cross sections at 10 meV for the ^{3}HeT($v = 0, j = 0$)$^+$ ground state. See DOI: https://doi.org/10.1039/d5cp03908h.

Acknowledgements

This work has been supported by the Ministerio de Ciencia, Innovación y Universidades with Grant No. MICIU/AIE/10.13039/501100011033 PID2024-155666NB-I00. Y. S., D. B. and J. S. thank support from the High Performance Computing Platform MESO@LR at the University of Montpellier.

References

1 M. Aker and K. Altenmüller, *et al.*, *Phys. Rev. Lett.*, 2019, **123**, 221802.
2 A. Aker and A. Beglarian, *et al.*, *Nat. Phys.*, 2022, **18**, 160–166.
3 J. Kellerer and F. Spanier, *J. Instrum.*, 2022, **17**, P06029.
4 C. Sendlinger, J. Kellerer and F. Spanier, *arXiv*, 2025, preprint, arXiv:2503.10263, DOI: 10.48550/arXiv.2503.10263.
5 A. Ashtari Esfahani, S. Böser, *et al.*, *arXiv*, 2022, preprint, arXiv:2203.07349, DOI: 10.48550/arXiv.2203.07349.
6 J. Sahoo, D. Bossion, T. González-Lezana, D. Talbi and Y. Scribano, *J. Chem. Phys.*, 2024, **161**, 144312.
7 J. Lv, X. Liu, J. Liang and H. Sun, *Can. J. Phys.*, 2010, **88**, 899–904.
8 J. Liang, X. Liu, W. Xu, H. Kong and Q. Zhang, *J. Mol. Struct.: THEOCHEM*, 2010, **942**, 93–97.
9 S. Bovino, M. Tacconi, F. A. Gianturco and D. Galli, *Astron. Astrophys.*, 2011, **529**, A140.
10 S. Bovino, M. Tacconi and F. A. Gianturco, *J. Phys. Chem. A*, 2011, **115**, 8197–8203.
11 S. Bovino, F. Gianturco and M. Tacconi, *Chem. Phys. Lett.*, 2012, **554**, 47–52.
12 D. De Fazio, *Phys. Chem. Chem. Phys.*, 2014, **16**, 11662–11672.
13 P. Gamallo, S. Akpinar, P. Defazio and C. Petrongolo, *J. Phys. Chem. A*, 2014, **118**, 6451–6456.
14 F. Esposito, C. M. Coppola and D. De Fazio, *J. Phys. Chem. A*, 2015, **119**, 12615–12626.
15 T. González-Lezana, D. Bossion, Y. Scribano, S. Bhowmick and Y. V. Suleimanov, *J. Phys. Chem. A*, 2019, **123**, 10480–10489.
16 C. Ramachandran, D. De Fazio, S. Cavalli, F. Tarantelli and V. Aquilanti, *Chem. Phys. Lett.*, 2009, **469**, 26–30.
17 F. Grussie, J. Sahoo, Y. Scribano, D. Bossion, L. Berger, M. Grieser, L. W. Isberner, A. Kálosi, O. Novotný, D. Paul, A. Znotins, X. Urbain and H. Kreckel, *Astron. Astrophys.*, 2025, **699**, L12.
18 M. Upadhyay, S. Kässer, J. Sahoo, Y. Scribano and M. Meuwly, *Precis. Chem.*, 2025, **3**, 677.
19 H. Werner and P. J. Knowles, *J. Chem. Phys.*, 1988, **89**, 5803.
20 P. J. Knowles and H. Werner, *Chem. Phys. Lett.*, 1988, **145**, 514.
21 P. Knowles and N. Handy, *Chem. Phys. Lett.*, 1984, **111**, 315.
22 P. J. Knowles and N. C. Handy, *Comput. Phys. Commun.*, 1989, **54**, 75.
23 T. H. Dunning, Jr, *J. Chem. Phys.*, 1989, **90**, 1007.
24 A. Aguado and M. Paniagua, *J. Chem. Phys.*, 1992, **96**, 1265.
25 D. Koner, J. C. San Vicente Veliz, A. van der Avoird and M. Mewley, *Phys. Chem. Chem. Phys.*, 2019, **21**, 24976.
26 D. Skouteris, J. F. Castillo and D. E. Manolopoulos, *Comput. Phys. Commun.*, 2000, **133**, 128–135.
27 D. E. Manolopoulos, *J. Chem. Phys.*, 1986, **85**, 6425–6429.
28 E. J. Rackham, F. Huarte-Larranaga and D. E. Manolopoulos, *Chem. Phys. Lett.*, 2001, **343**, 356–364.
29 E. J. Rackham, T. González-Lezana and D. E. Manolopoulos, *J. Chem. Phys.*, 2003, **119**, 12895.
30 T. González-Lezana, *Int. Rev. Phys. Chem.*, 2007, **26**, 29.
31 D. G. Truhlar and J. T. Muckerman, in *Reactive Scattering Cross Sections III: Quasiclassical and Semiclassical Methods*, ed. R. B. Bernstein, Springer US, Boston, MA, 1979, pp. 505–566.
32 C. C. Marston and G. G. Balint-Kurti, *J. Chem. Phys.*, 1989, **91**, 3571–3576.
33 M. V. Berry and K. E. Mount, *Rep. Prog. Phys.*, 1972, **35**, 315–397.
34 D. Manolopoulos, *J. Chem. Soc., Faraday Trans.*, 1997, **93**, 673.
35 R. Martínez, M. Paniagua, J. Mayneris-Perxachs, P. Gamallo and M. González, *Phys. Chem. Chem. Phys.*, 2017, **19**, 3857.
36 T. González-Lezana, O. Roncero, P. Honvault, J.-M. Launay, N. Bulut, F. J. Aoiz and L. Bañares, *J. Chem. Phys.*, 2006, **125**, 094314.

